

A Solid Chelating Ligand: Periodic Mesoporous Organosilica Containing 2,2'-Bipyridine within the Pore Walls

Minoru Waki,^{†,∇,◆} Yoshifumi Maegawa,^{†,‡,∇} Kenji Hara,^{‡,§} Yasutomo Goto,^{†,‡} Soichi Shirai,^{†,‡} Yuri Yamada,^{†,‡} Norihiro Mizoshita,[†] Takao Tani,[†] Wang-Jae Chun,[⊥] Satoshi Muratsugu,^{||} Mizuki Tada,[#] Atsushi Fukuoka,[§] and Shinji Inagaki^{*,†,‡}

[†]Toyota Central R&D Laboratories, Inc. and [‡]Japan Science and Technology Agency (JST)/ACT-C, Nagakute, Aichi 480-1192, Japan

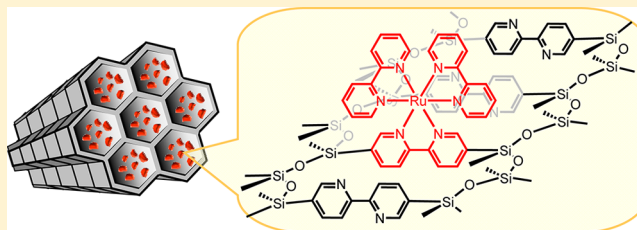
[§]Catalysis Research Center, Hokkaido University, Sapporo 001-0021, Japan

[⊥]Graduate School of Arts and Sciences, International Christian University, Mitaka, Tokyo 181-8585, Japan

^{||}Department of Chemistry, Graduate School of Science and [#]Research Center for Materials Science, Nagoya University, Furo-cho, Chikusa, Nagoya 464-8602, Japan

Supporting Information

ABSTRACT: Synthesis of a solid chelating ligand for the formation of efficient heterogeneous catalysts is highly desired in the fields of organic transformation and solar energy conversion. Here, we report the surfactant-directed self-assembly of a novel periodic mesoporous organosilica (PMO) containing 2,2'-bipyridine (bpy) ligands within the framework (BPy-PMO) from a newly synthesized organosilane precursor [(*i*-PrO)₃Si-C₁₀H₆N₂-Si(O*i*-Pr)₃] without addition of any other silane precursors. BPy-PMO had a unique pore-wall structure in which bipyridine groups were densely and regularly packed and exposed on the surface. The high coordination ability to metals was also preserved. Various bipyridine-based metal complexes were prepared using BPy-PMO as a solid chelating ligand such as Ru(bpy)₂(BPy-PMO), Ir(ppy)₂(BPy-PMO) (ppy = 2-phenylpyridine), Ir(cod)(OMe)(BPy-PMO) (cod = 1,5-cyclooctadiene), Re(CO)₃Cl(BPy-PMO), and Pd(OAc)₂(BPy-PMO). BPy-PMO showed excellent ligand properties for heterogeneous Ir-catalyzed direct C–H borylation of arenes, resulting in superior activity, durability, and recyclability to the homogeneous analogous Ir catalyst. An efficient photocatalytic hydrogen evolution system was also constructed by integration of a Ru-complex as a photosensitizer and platinum as a catalyst on the pore surface of BPy-PMO without any electron relay molecules. These results demonstrate the great potential of BPy-PMO as a solid chelating ligand and a useful integration platform for construction of efficient molecular-based heterogeneous catalysis systems.



INTRODUCTION

A variety of functional systems based on metal complexes with chelating ligands have been constructed for applications such as catalysis for organic synthesis¹ and photosensitizers for photoreaction systems.² For practical applications, immobilization of metal complexes on solid supports is important for easy recovery and recycle uses and allows easy integration of different components for constructing highly functional systems.³ There are some successful examples for heterogenized metal complex showing comparable or superior catalytic performance to the homogeneous analogue.³ However, immobilization on conventional supports such as silica gel has often resulted in decreases in the performances of metal complexes, such as catalytic activity and selectivity, because the uniform environment of the homogeneous metal complexes is disturbed by unfavorable interactions with the solid surface and nonuniform fixation on the surface.⁵ Moreover, the diffusion limitation of substrate and product molecules has been a problem for porous supports due to a decrease in reaction

efficiency in their narrow channels. Thus, the development of a new support preserving the inherent functions of metal complexes is still a challenge for realizing their practical applications.

Ordered mesoporous materials, synthesized by a surfactant-directed self-assembly approach, are ideal supports due to their high surface areas and uniform mesopores for facile diffusion of molecules and ions. Periodic mesoporous organosilicas (PMOs), synthesized from organic-bridged silane precursors {R-[Si(X)₃]_n, n ≥ 2, R = organic group, X = OMe, OEt, O*i*-Pr, allyl}, are especially promising because functional organic groups can be incorporated into the framework without plugging the mesopore space, in contrast to mesoporous silicas functionalized with organic groups grafted on the pore surface.⁶ PMOs with a variety of organic groups in the frameworks have already been synthesized, including organic groups having

Received: December 27, 2013

Published: February 26, 2014

metal ligand abilities.^{7,8} Recently, we reported the synthesis of crystal-like PMOs containing divinylpyridine⁹ and phenylpyridine groups¹⁰ in the frameworks from 100% organosilane precursors of $(\text{EtO})_3\text{Si}-\text{C}_2\text{H}_2-\text{C}_5\text{H}_3\text{N}-\text{C}_2\text{H}_2-\text{Si}(\text{OEt})_3$ and $(\text{EtO})_3\text{Si}-\text{C}_6\text{H}_4-\text{C}_5\text{H}_3\text{N}-\text{Si}(\text{OEt})_3$, respectively. These pyridine-based PMOs have a crystal-like pore wall structure in which the pyridine moieties are densely and regularly arranged in the pore walls to form well-defined pore surface structures. The phenylpyridine-PMO was successfully utilized as a solid chelating ligand for the formation of metal complexes (ruthenium and iridium) on the pore surface by postsynthetic cyclometalation.^{10,11}

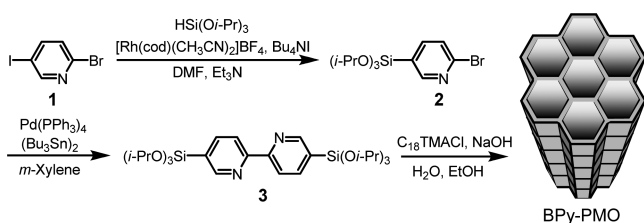
2,2'-Bipyridine is the most widely used chelating ligand for forming metal complexes in coordination and supramolecular chemistry.^{12,13} Although there have been several reports on the synthesis of mesoporous silicas¹⁴ or PMOs¹⁵ containing 2,2'-bipyridine ligands, they possessed a nonuniform pore surface structure due to the amorphous pore walls in which 2,2'-bipyridine groups were randomly distributed on the pore surface or in the walls. The amorphous pore walls resulted from the use of 2,2'-bipyridine precursors attached by one or two trialkoxysilyl groups via linkers such as alkyl chains, amides, or thioethers. Thus, the formation of crystal-like pore wall structures has been limited to PMOs synthesized from rigid bridging organics such as benzene,¹⁶ biphenyl,¹⁷ naphthalene,¹⁸ divinylbenzene,¹⁹ divinylpyridine,⁹ and phenylpyridine¹⁰ attached to two silyl groups but no linkers. We envisaged that a new precursor with a 2,2'-bipyridine directly attached to two silyl groups would be essential for the synthesis of crystal-like bipyridine-PMO.

Here, we report the successful synthesis of the crystal-like bipyridine-PMO (BPy-PMO) from 100% organosilane precursor $[(i\text{-PrO})_3\text{Si}-\text{C}_{10}\text{H}_6\text{N}_2-\text{Si}(\text{O}i\text{-Pr})_3]$. BPy-PMO had a well-defined pore surface structure where 2,2'-bipyridines were densely and regularly arranged and preserved the high coordination ability to metals. A variety of bipyridine-based metal complexes including iridium (Ir), ruthenium (Ru), rhenium (Re), and palladium (Pd) were easily formed on the pore surface. Furthermore, we discovered the excellent ligand properties of BPy-PMO in heterogeneous Ir-catalyzed direct C–H borylation of arenes with bis(pinacolato)diboron²⁰ and in heterogeneous photocatalytic hydrogen evolution from water using a Ru-complex and platinum integrated on the pore surface.

RESULTS AND DISCUSSION

Synthesis of Crystal-Like BPy-PMO from 100% Organosilane Precursor. The bipyridine precursor was prepared in two steps from a commercially available reagent. As shown in Scheme 1, 2-bromo-5-iodopyridine (**1**) was

Scheme 1. Synthesis of 5,5'-Bis(triisopropoxysilyl)-2,2'-bipyridine and Preparation of BPy-PMO through Hydrolysis and Polycondensation under Basic Conditions



silylated with triisopropoxysilane to give 2-bromo-5-(triisopropoxysilyl)pyridine (**2**), followed by Stille coupling of **2** with bis(tributyltin) to successfully afford 5,5'-bis(triisopropoxysilyl)-2,2'-bipyridine (**3**). Although methoxysilyl or ethoxysilyl groups have been widely employed as organosilane precursors for the synthesis of PMOs and silica-based sol–gel materials, they have low tolerance for many organic reactions and are difficult to purify due to their high reactivity. In contrast, the isopropoxysilyl group was stable enough to allow several reactions using organometallic reagents and purification by silica gel chromatography.²¹ The use of the isopropoxysilyl group led to easy synthesis of the bipyridine precursor directly attached to two alkoxyisilyl groups **3**.

BPy-PMO was prepared by hydrolysis and polycondensation from precursor **3** under basic conditions in the presence of octadecyltrimethylammonium chloride ($\text{C}_{18}\text{TMACl}$) surfactant as a structure directing agent, followed by extraction of the surfactant with an acidic ethanol solution (Scheme 1). Strongly basic conditions (0.25 M) with aging at 95 °C caused cleavage of the Si–C bond in the bipyridine precursor (Figure S1). The Si–C bond cleavage was very sensitive to basicity and temperature due to the localization of electrons at the nitrogen atoms and the resulting deficiency of electrons in the pyridine rings, which was predicted from theoretical studies on Si–C cleavage in organosilane precursors during the condensation process.²² However, at weak basicity (0.005 M) and room temperature, the hydrolysis of the isopropoxysilyl groups was found to be slow, which was attributed to the low nucleophilicity of hydroxide for attacking the bulky isopropoxy group. Consequently, the synthesis was carried out under moderately basic conditions of 0.035 M and 50 °C with a long aging time (6 days), which successfully afforded highly ordered BPy-PMO powder. The ¹³C cross-polarization (CP) magic-angle-spinning (MAS) NMR, ²⁹Si MAS NMR and FT-IR spectra confirmed the preservation of both the bipyridine moieties and Si–C bonds during the synthesis and extraction processes (Figures 1a–c and S2). The ¹³C CP MAS NMR spectrum displayed the five aromatic resonances similar to ¹³C NMR spectrum of precursor **3**, which can be assigned to carbons on the pyridine ring. The ²⁹Si MAS NMR spectrum showed T² [$\text{SiC}(\text{OSi})_2(\text{OH})$] and T³ [$\text{SiC}(\text{OSi})_3$] signals, but almost no Qⁿ [$\text{Si}(\text{OSi})_n(\text{OH})_{4-n}$, $n = 2-4$] signals between –90 and –120 ppm, indicating almost complete preservation of Si–C bonds (Figure 1c). The presence of T² signal also shows that a considerable amount of silanol groups exist in BPy-PMO. During optimization of the synthetic conditions, slow addition of the precursor solution was found to be crucial to prepare well-ordered BPy-PMO. Thus, the precursor solution was slowly added over a period of 3 h at a constant speed using a syringe pump (Figure S5). Fast addition of the precursor caused the aggregation of precursor molecules in aqueous reaction media due to the slow hydrolysis rate of isopropoxysilyl groups, which resulted in the formation of disordered material.

The XRD patterns of surfactant-free BPy-PMO showed low angle reflections at $2\theta = 1.96^\circ$, 3.40° , and 3.84° (d spacings of 4.50, 2.60, and 2.30 nm, respectively) corresponding to a two-dimensional hexagonal lattice ($a_0 = 5.2$ nm), and four other peaks at a medium scattering angle of $7-23^\circ$ (d spacings of 1.16, 0.58, and 0.39 nm), corresponding to a lamellar structure with a molecular-scale periodicity of bipyridine and silica moieties in the pore walls (Figure 1d). The broad peak at $2\theta = 18-25^\circ$ was due to disordered arrangement of atoms in the

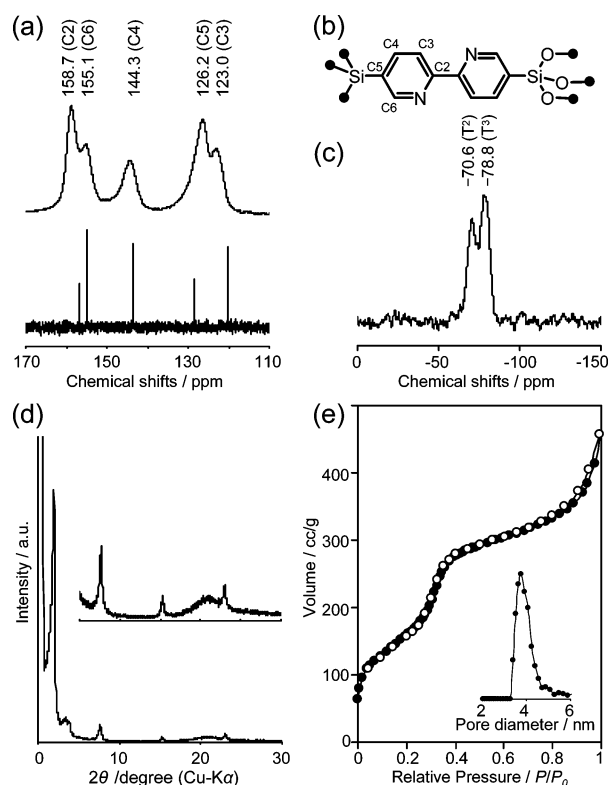


Figure 1. (a) ^{13}C CP MAS NMR spectrum of BPy-PMO (above) and ^{13}C NMR spectrum of precursor **3** (below). (b) Numbering system of bipyridine. (c) ^{29}Si MAS NMR spectrum, (d) XRD patterns, and (e) nitrogen adsorption/desorption isotherms for BPy-PMO.

silica belt-like layers shown later, but not due to amorphous regions or contamination of amorphous materials. The nitrogen adsorption/desorption isotherms showed a type-IV isotherm, typical of ordered mesoporous materials (Figure 1e). The density functional theory pore diameter (d_{DFT}), Brunauer–Emmett–Teller surface area (S_{BET}) and pore volume were 3.8 nm, 739 m^2g^{-1} , and 0.41 cm^3g^{-1} , respectively. The pore wall thickness was estimated to be 1.4 nm ($a_0 - d_{\text{DFT}}$), corresponding to three layers of the bipyridine moieties in the pore walls.

Figure 2a–d shows the scanning and transmission electron microscopy (SEM and TEM) images of BPy-PMO. The SEM image showed particle morphology with diameters of 200–500 nm (Figure 2a). The TEM images showed one-dimensional channels going through the particles, indicating that the particles have a single crystal-like structure (Figure 2b). The enlarged TEM images showed a hexagonal arrangement of uniform pores (Figure 2c) and many lattice fringes with a basal spacing of ca. 1.2 nm in the perpendicular direction to the mesochannels (Figure 2d), which was in good agreement with the result obtained by XRD. Figure 2e shows a structural model of BPy-PMO. The bipyridine and silica belt-like layers in the walls are arranged alternatively with a periodicity of 1.16 nm in the channel direction whose periodicity was clearly observed by XRD and TEM (Figures 1d and 2d). A molecular mechanics simulation showed that the neighboring bipyridine–bipyridine distance is approximately 0.44 nm, which is larger than the usual π – π stacking distance of aromatic compounds, although the molecular arrangement and intermolecular distance can fluctuate due to the flexibility of the silica framework. The loosely packed bipyridine groups could have a high degree of

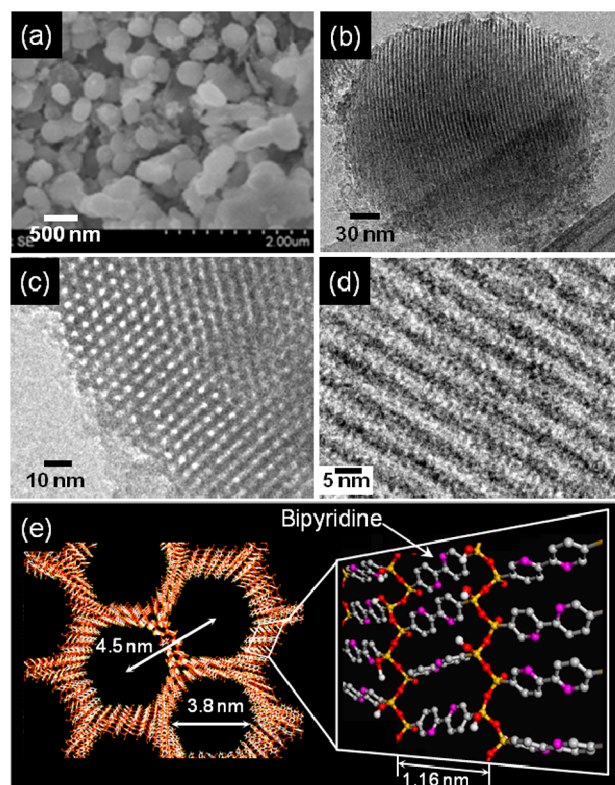


Figure 2. (a) SEM and (b–d) TEM images and (e) structural model of BPy-PMO. Silicon, yellow; oxygen, red; carbon, gray; nitrogen, pink; hydrogen, white. Hydrogen on bipyridine is omitted.

freedom to rotate about the Si–C axis because rotary motion of the bridging organic groups in crystal-like benzene- and biphenyl-PMOs with similar packing structures has been demonstrated by NMR spectroscopy.²³ It is suggested that the framework bipyridine groups preserved their coordination ability for metal complex formation.

Elemental analysis of carbon and nitrogen in BPy-PMO gave a carbon/nitrogen ratio of 4.5, which is consistent with that expected from the chemical formula ($\text{C}_{10}\text{H}_6\text{N}_2$) of the bipyridine bridges. The amount of bipyridine moieties in BPy-PMO was estimated from the nitrogen content as 3.18 mmol g^{-1} . Thermogravimetric analysis showed that weight loss due to decomposition of the BPy moieties occurred in the temperature range of 500–600 $^{\circ}\text{C}$ with a maximum at 570 $^{\circ}\text{C}$, showing high thermal stability up to 500 $^{\circ}\text{C}$ due to the robust siloxane bond network (Figure S4).

Metal Complex Formations using BPy-PMO as a Ligand. A variety of bipyridine-based metal complexes can be readily formed on the pore surface of BPy-PMO by simple stirring of the BPy-PMO powder in a solution containing a metal precursor (Figure 3).

$\text{Ru}(\text{bpy})_2(\text{BPy-PMO})$ was formed by dispersion of BPy-PMO powder in ethanol solution containing $\text{Ru}(\text{bpy})_2\text{Cl}_2 \cdot 2\text{H}_2\text{O}$ precursor (Figure S9).²⁴ The UV–vis diffuse reflectance spectrum of the obtained powder showed a broad band at around 450 nm due to metal-to-ligand charge transfer (MLCT) and an intense peak at around 300 nm due to π – π^* transition of ligands, which was very similar to the absorption spectrum of a homogeneous solution of $\text{Ru}(\text{bpy})_3\text{Cl}_2$ except for peak broadening (Figure 4a).²⁵ The peak broadening suggests a slight difference in the electronic state of $\text{Ru}(\text{bpy})_2(\text{BPy-PMO})$ from its homogeneous analogue because one of the bipyridine

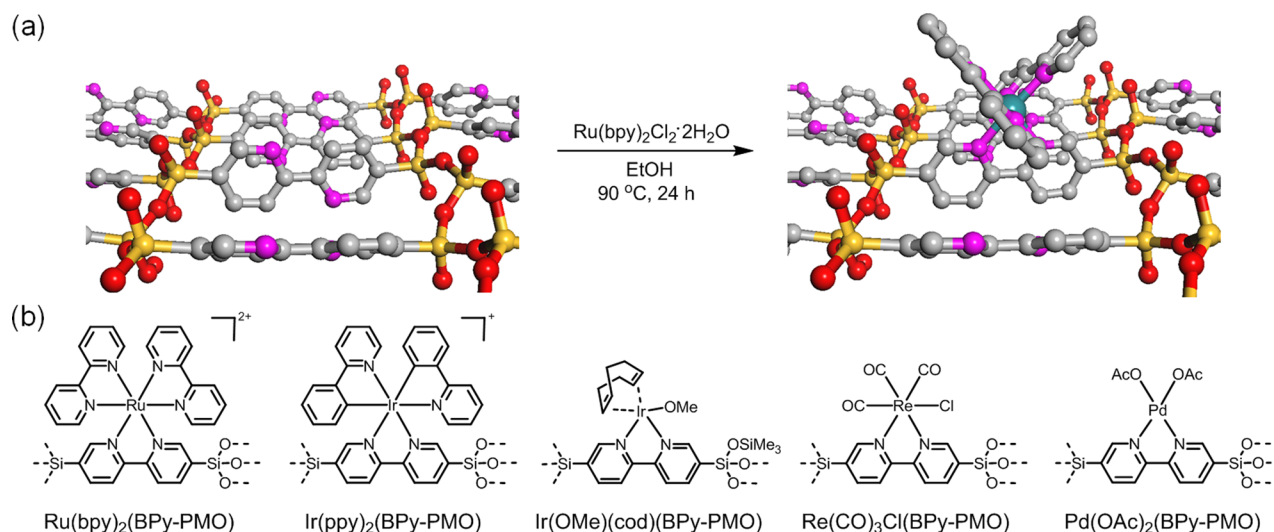


Figure 3. (a) CG image of the direct Ru-complex formation on the pore surface of BPy-PMO. Green, ruthenium. The other colors correspond to those in Figure 2. (b) Chemical structures of metal complexes prepared using BPy-PMO as a solid chelating ligand in this study.

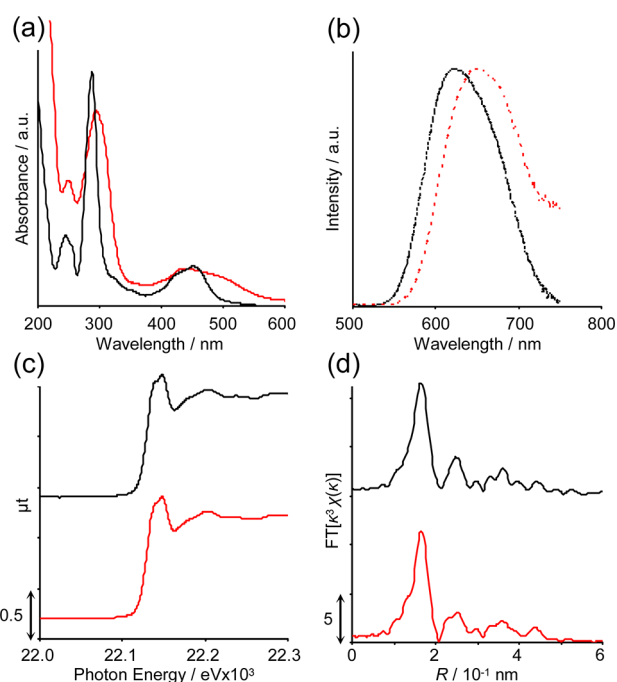


Figure 4. (a) UV-vis absorption, (b) photoluminescence, (c) Ru *K*-edge XANES spectra, and (d) EXAFS Fourier transform ($\kappa = 30\text{--}140\text{ nm}^{-1}$) of Ru(bpy)₂(BPy-PMO) (red line) and Ru(bpy)₃Cl₂ (black line).

ligands was covalently fixed in the PMO framework by silicon atoms at the *S,S'*-positions.²⁶ This was also suggested by the slightly different emission band from that of the homogeneous one (Figure 4b). A detailed investigation on this difference is currently underway in our laboratory. The X-ray absorption fine structure (XAFS) measurement was also carried out to elucidate the structure of the Ru center in the pore walls (Figure 4c,d). The X-ray absorption near edge spectroscopy (XANES) spectrum and extended X-ray absorption fine structure (EXAFS) Fourier transform at Ru *K*-edge showed spectral characteristics corresponding to those of homogeneous Ru(bpy)₃Cl₂, suggesting successful formation of [Ru(bpy)₃]²⁺ complex on the pore surface of BPy-PMO (Figure S10).

Ir(ppy)₂(BPy-PMO) was prepared by reaction with [Ir(ppy)₂Cl]₂ in CH₂Cl₂.²⁷ The UV-vis diffuse reflectance spectrum showed an absorption band of MLCT at 378 nm with a long tail above 450 nm. The tail was attributed to a direct spin-forbidden absorption from the singlet ground state to triplet excited state as observed for [Ir(C[∧]N)₂(N[∧]N)]⁺, where (C[∧]N) and (N[∧]N) indicate a cyclometalating ligand such as 2-phenylpyridine and a neutral ligand such as 2,2'-bipyridine (Figure S12).²⁷ The emission of Ir(ppy)₂(BPy-PMO) was also observed at a similar wavelength for the homogeneous analogue (Figure S13).^{27b}

Ir(cod)(OMe)(BPy-PMO) was synthesized by treating an end-capped BPy-PMO with [Ir(OMe)(cod)]₂ precursor in benzene (Figure S15). The end-capped BPy-PMO was prepared by trimethylsilylation of surface silanol groups with *N*-trimethylsilylimidazole for application to catalysis (see Supporting Information, section 3). XANES spectrum and EXAFS Fourier transform at Ir *L*_{III} edge of the PMO were in good agreement with those of the homogeneous complex [Ir(OMe)(cod)(bpy)] (Figure S16). The X-ray photoelectron spectroscopy (XPS) spectra of the PMO displayed almost the same binding energies of 61.3 eV for Ir 4f_{7/2} and 64.5 eV for Ir 4f_{5/2} as the homogeneous analogue (Figure S17). These results suggest successful formation of Ir(cod)(OMe)(BPy-PMO).

Re(CO)₃Cl(BPy-PMO) was prepared by treatment with Re(CO)₅Cl in toluene.²⁸ The UV-vis spectrum of Re(CO)₃Cl(BPy-PMO) showed an MLCT absorption band (around 390 nm) assignable to the coordination of Re to bpy ligand (Figure S19).²⁶ In the FT-IR spectrum of the Re complex, three characteristic CO stretching bands were observed at 1893, 1920, and 2023 cm⁻¹, which is in good agreement with those of Re(bpy)(CO)₃Cl (Figure S20).²⁹ The XAFS measurement also suggested the formation of the desired Re complex in the PMO material (Figure S21).

Pd(OAc)₂(BPy-PMO) was obtained by reaction with Pd(OAc)₂ in THF.³⁰ The UV-vis diffuse-reflectance spectrum of the PMO showed the appearance of a shoulder band around 370 nm, suggesting that Pd(II) directly interacts with BPy groups in the PMO framework without formation of Pd black (Figure S23). The formation of Pd(OAc)₂(BPy-PMO) was also confirmed by XPS investigation. As shown in Figure S24, the

binding energy of Pd 3d_{5/2} in the PMO is 337.0 eV, indicating the strong coordination of BPy groups in PMO to Pd(II) species. The observed binding energy is lower than that of 337.5 eV for free Pd(OAc)₂, suggesting that the electron-donating character of BPy induced a negative shift in binding energy for the Pd species.³¹

The loading amounts of metals on BPy-PMO were determined by inductively coupled plasma (ICP)-atomic emission spectrometry (AES) and are listed in Table 1. The

Table 1. Physical Parameters of Metal Complexes Prepared Using BPy-PMO

metal-BPy-PMO	loading of metal mmol/g	metal/bpy	S _{BET} m ² /g	d _{DFT} nm
Ru(bpy) ₂ (BPy-PMO)	0.20	0.071	530	3.2
Ir(ppy) ₂ (BPy-PMO)	0.26	0.095	700	3.1
Ir(OMe)(cod)(BPy-PMO)	0.16	0.056	520	3.5
Re(CO) ₃ Cl(BPy-PMO)	1.12	0.56	500	3.2
Pd(OAc) ₂ (BPy-PMO)	0.74	0.28	580	3.4
BPy-PMO	—	—	740	3.8

amounts of metals were 0.16–1.12 mmol g⁻¹, which indicated that 7–56% of bipyridine groups in BPy-PMO were coordinated to metals. The large differences in the loading amounts of metals may be explained by the bulkiness of free ligands (Figure 3b) or the reactivity of BPy-PMO with each metal complex precursor. However, the loading amounts can be controlled to some extent by conditions such as concentration of metal precursors in the treated solution. The XRD patterns and nitrogen adsorption/desorption isotherms for BPy-PMOs after the formation of metal complexes showed almost complete preservation of the ordered mesoporous structure and molecular scale periodicity, indicating high chemical stability of BPy-PMO (see Supporting Information, section 4). In addition, the metal-BPy-PMOs still have large mesopores of 3.1–3.8 nm and high surface areas of 500–740 m² g⁻¹ (Table 1).

The above results clearly indicate the great potential of BPy-PMO as a chelating ligand for the formation of a variety of solid-state bipyridine-based metal complexes with high surface areas. The metal complex-BPy-PMOs have the potential to show good catalytic performance similar to their homogeneous analogues because of the well-defined catalytic centers on the surface and efficient mass transportation due to the large mesopores. Furthermore, the high stability of BPy-PMO could allow easy separation and recycle use of the heterogeneous metal catalysts.

Solid Ligand Properties for Direct C–H Borylation of Arenes. Construction of isolated and well-defined catalytic active centers onto solid supports is a subject of central importance in the development of efficient heterogeneous molecular catalysts.³² In homogeneous catalysis, the Ir-bipyridine complex was found to show both high catalytic activity and functional tolerance for direct C–H borylation of arenes, one of the most important transformations for preparing useful aryl boryl ester intermediates.³³ To date, heterogeneous molecular catalysts for C–H borylation have been limited to the Ir-silica-supported phosphine complex³⁴ and polymeric Ir-bipyridine complex catalysts.³⁵ Herein, BPy-PMO was used as a solid chelating ligand for the heterogeneous Ir-catalyst for direct C–H borylation of arenes.

Direct C–H borylation was carried out in the presence of Ir(OMe)(cod)(BPy-PMO) (denoted by Ir-PMO in this section, 0.75 mol % Ir) and bis(pinacolato)diboron (B₂pin₂) (0.33 mmol) in arenes (20 mmol) at 80 °C for 12 h. The catalytic activity was compared to those of a homogeneous iridium catalyst with a molecular bipyridine ligand and heterogeneous iridium catalysts with bipyridine ligands grafted on silica gel (L1), mesoporous silica (L2), and polystyrene (L3). Ir-PMO catalyzed the direct C–H borylation of benzene and gave the desired product in high yield of 94%, which was higher than those obtained with a homogeneous catalyst (80%) and grafted catalysts on silica gel (33%) and mesoporous silica (63%). The grafted catalyst on polystyrene showed no catalytic activity.

In order to elucidate the catalytic behavior, the reaction kinetics were studied as shown in Figure 5a. The PMO catalyst

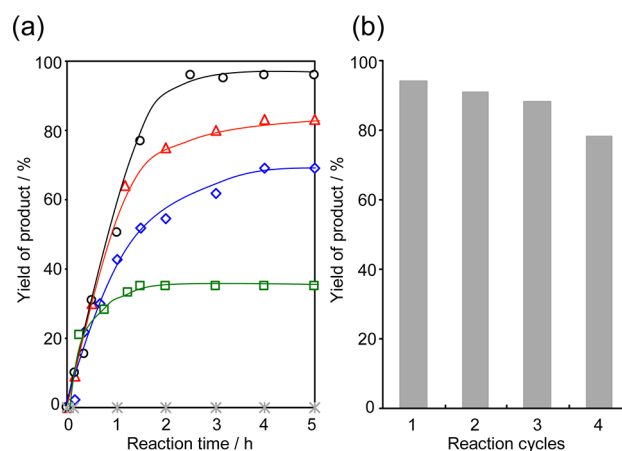
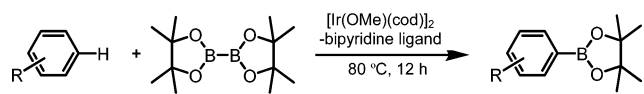


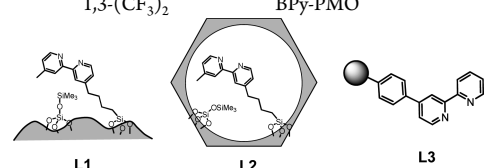
Figure 5. (a) Reaction kinetic curves of C–H borylation of benzene catalyzed by iridium catalysts based on BPy-PMO (black line), 2,2'-bipyridine (red line), L1 (blue line), L2 (green line), and L3 (gray line). (b) Reusability of recovered PMO catalyst, first cycle (original: 94%), second cycle (91%), third cycle (88%), and fourth cycle (78%).

retained its activity until the end of the reaction, while the reaction rates of homogeneous and grafted iridium complexes decreased within 2 h. The decreased grafted reaction rates indicate deactivation of the active center possibly due to aggregation of the iridium species and/or undesired interaction between the active center and solid surface. These results suggest that BPy-PMO is an effective solid ligand for suppression of aggregation and undesired interactions of the metal center due to the isolate binding of metals on the well-defined surface. It is noteworthy that the initial reaction rate for Ir-PMO is almost the same as that of the homogeneous catalyst with the same amount of Ir. This result suggests a very small diffusion limitation of molecules (B₂pin₂, products, etc.) in the mesochannels due to the large pore size. The grafted mesoporous silica showed a slightly lower initial reaction rate than Ir-PMO, possibly due to the effect of the protruded iridium complexes into the mesochannels. The grafted silica gel showed an initial reaction rate similar to that of Ir-PMO because of the large mean pore diameter (6.3 nm) of the silica gel (Figure S26).

The scope of this system was then examined using various types of substrates (Table 2, entries 6–12). Ir-PMO catalyzed C–H borylation of both electron-rich and -poor substituted arenes. In the case of monosubstituted arenes, the reaction gave regioisomeric mixtures of the *meta*- and *para*-borylation

Table 2. Ligand Effects in Ir-Catalyzed Direct C–H Borylation of Arenes with B₂pin₂


entry	R	ligand	yield (%) ^a
1	H	BPy-PMO	94
2	H	2,2'-bipyridine	80
3	H	L1	33
4	H	L2	63
5	H	L3	0
6	CH ₃	BPy-PMO	85 ^b
7	OMe	BPy-PMO	88 ^c
8	CO ₂ Me	BPy-PMO	88 ^d
9	1,2-(CH ₃) ₂	BPy-PMO	60
10	1,2-Cl ₂	BPy-PMO	92
11	1,3-Cl ₂	BPy-PMO	81
12	1,3-(CF ₃) ₂	BPy-PMO	47



^aIsolated yield of aryl boronate based on boron atom in B₂pin₂. ^bm:p = 63:37. ^cm:p = 63:37. ^dm:p = 56:44.

products (Table 2, entries 6–8). In contrast, regioselective borylation was observed for disubstituted arenes. Both 1,2- and 1,3-disubstituted arenes yielded the corresponding boronate esters as single regioisomers due to steric hindrance of the substituents (Table 2, entries 9–12). Similar behaviors were observed for the homogeneous system.³²

The PMO catalyst was easily recovered by simple filtration and was available for recycle use (Figure 5b). The recovered PMO catalyst retained good catalytic activity with slight loss of product yield for at least three cycles. In contrast, the homogeneous and the grafted catalysts showed almost no catalytic activity for recycle use, indicating almost complete deactivation during the first reaction cycle. These results indicate good recyclability of the Ir-PMO catalyst.

Finally, a hot-filtration experiment was conducted to check the catalytic activity of leached Ir species. After the reaction had proceeded for 1 h with a yield of 54%, the PMO catalyst was filtered by using a membrane filter (0.20 μm) under argon, and the resulting transparent solution was allowed to react under identical conditions for another 23 h (Figure S27). No significant change in the product yield was observed, indicating that the reaction completely stopped. ICP analysis showed that the concentration of Ir species in the filtrate was under the detection limit (1 ppm). These results clearly indicate that the catalytic reaction occurred by the iridium complex fixed on BPy-PMO without leaching of Ir species.

A Platform for Integrated Heterogeneous Photocatalytic Hydrogen Evolution System. BPy-PMO is also expected to be a useful platform with which to integrate different functional components for construction of efficient solar energy conversion systems. [Ru(bpy)₃]²⁺ is a typical photosensitizer which has been widely applied to homogeneous and heterogeneous photocatalysis systems such as photocatalytic hydrogen evolution from water in the presence of platinum (as a catalyst), methylviologen (as an electron

mediator), and as a sacrificial reducing agent.³⁶ In this work, we have constructed a heterogeneous photocatalytic hydrogen evolution assembly of BPy-PMO integrated with a [Ru(bpy)₃]²⁺ photosensitizer and platinum catalyst on the pore surface without any electron mediators such as methylviologen as shown in Figure 6a.

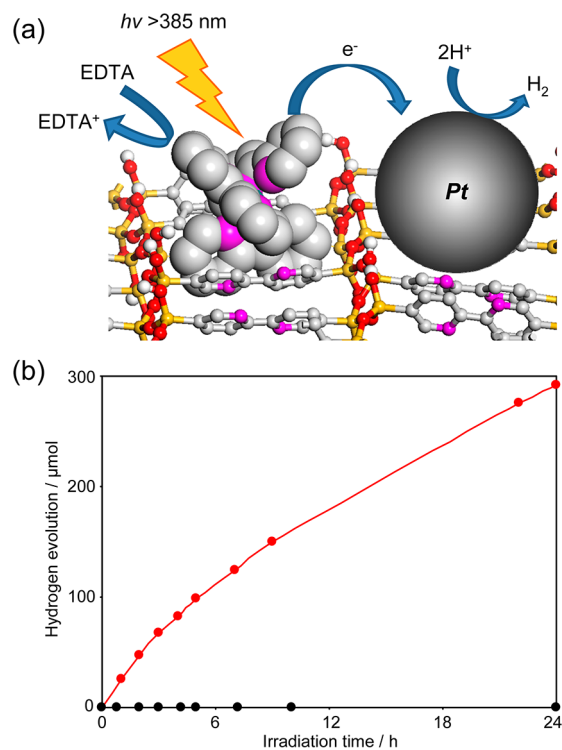


Figure 6. (a) Schematic illustration of a hydrogen evolution system based on Pt/Ru-PMO. Ru-complex is represented as a CPK model. (b) Time-dependent hydrogen evolution curves of Pt/Ru-PMO (red line) and homogeneous Ru(bpy)₃Cl₂ and colloidal platinum particles system (black line) under irradiation of visible light (>385 nm).

Ru(bpy)₂(BPy-PMO) (denoted by Ru-PMO in this section) was loaded with Pt by stirring in an aqueous Pt(IV) salt solution at 80 °C (Figure S29). The loading amount of Pt was 1.10 mmol g⁻¹, which was determined by ICP analysis. TEM revealed the formation of many small nanoparticles with diameters of 2–3 nm in the PMO particles (Figure S30). The XRD pattern exhibited very broad peaks at *d* = 0.22 and 0.19 nm corresponding to (111) and (200) faces of the Pt crystal (Figure S31a).³⁷ These results indicate that Pt nanoparticles were supported on Ru-PMO, including inside the mesochannels, owing to the small sizes of the Pt nanoparticles.

The photocatalytic reaction was carried out using a Pyrex reaction vessel connected to a glass-enclosed gas circulation and evacuation system. Pt-loaded Ru-PMO was suspended in an acetate buffer solution containing EDTA as a sacrificial reducing agent in the vessel. Hydrogen was evolved continuously and steadily under irradiation of visible light (>385 nm). The amount of produced hydrogen reached 300 μmol after 24 h, corresponding to a Ru-based turnover number of 184.

This indicates that Ru-PMO can act as a photosensitizer for hydrogen evolution in combination with Pt nanoparticles without any electron mediators. Direct electron transfer from Ru complexes to Pt nanoparticles occurred in this system

because both components were fixed on the pore surface and were in constant contact with each other. As a control experiment, homogeneous Ru(bpy)₃Cl₂ and colloidal platinum particles were used instead of Pt-loaded Ru-PMO with the same Ru and Pt contents. The homogeneous system showed almost no hydrogen evolution (Figure 6b). However, the addition of methylviologen to the homogeneous system brought about evolution of a considerable amount of hydrogen. These results suggest that BPy-PMO acts a useful platform to integrate [Ru(bpy)₃]²⁺ and Pt on the pore surface and promotes efficient photoinduced electron transfer from the photosensitizer to the catalyst without any electron relay molecules.

CONCLUSIONS

A novel crystal-like PMO with a high density of bipyridine groups in the framework was successfully synthesized from a bipyridine-bridged organosilane precursor. BPy-PMO was demonstrated to act as a versatile chelating ligand for the formation of various bipyridine-based metal complexes on the pore surface due to the high coordination ability of the framework bipyridine ligands. BPy-PMO was successfully used in the heterogeneous Ir-catalyzed direct C–H borylation of arenes, which showed high activity similar to the corresponding homogeneous Ir-complex and high durability due to the suppression of Ir-complex aggregation on the pore surface. Ir-BPy-PMO allowed for easy recovery and recycle use and very low contamination of Ir in the final product. BPy-PMO was also a useful platform for construction of a heterogeneous molecular photocatalyst system. The integration of Ru(bpy)₃²⁺ photosensitizer and Pt catalyst on the pore surface exhibited catalytic hydrogen evolution from water without any electron mediators. These results demonstrate the great potential of BPy-PMO as a solid chelating ligand and an integration platform for a variety of molecular-based heterogeneous catalysis systems such as organic transformations and solar energy conversion.

EXPERIMENTAL SECTION

Materials and Methods. All reactions for organic synthesis were carried out under argon using standard high-vacuum and Schlenk-line techniques. Unless otherwise noted, all chemicals, including dry solvents, were purchased from commercial suppliers (Sigma-Aldrich, Tokyo Chemical Industry Co., Ltd., and Wako Pure Chemical Industries Ltd.) and used without further purification.

Mass spectra were recorded on a Micromass GCT Premier mass spectrometer (FI: field ionization) and Micromass Q-TOF mass spectrometer (ESI: electrospray ionization). ¹H, ¹³C, and ¹⁹F NMR spectra were obtained using a Jeol ECX-400 spectrometer operating at 400 MHz, 100 Hz, and 376 MHz, respectively. Chemical shifts are reported in δ parts per million referenced to tetramethylsilane (TMS) or residual protonated solvent as an internal standard. ²⁹Si dipolar decoupling (DD) and ¹³C cross-polarization (CP) MAS NMR measurements were respectively performed at 79.49 and 100.6 MHz at a sample spinning frequency of 4 or 6 kHz using a Bruker Avance 400 spectrometer with a 7 mm zirconia rotor. For the ²⁹Si MAS NMR measurements, the repetition delay was 60 s, and the pulse width was 4.5 μ s. For the ¹³C CP-MAS NMR measurements, the repetition delay was 5 s, the contact time was 1.75 ms, and the pulse width was 4.5 μ s (¹H 90° pulse). Chemical shifts were referenced to TMS and glycine for ²⁹Si and ¹³C NMR, respectively. XRD profiles were recorded on a Rigaku RINT-TTR diffractometer using Cu K α radiation (50 kV, 300 mV). Nitrogen adsorption and desorption isotherms were measured using a Quantachrome Nova3000e sorptometer. BET surface areas were calculated from the linear sections of BET plots ($P/P_0 = 0.1$ –

0.2). Pore-size distributions were calculated using the DFT method (DFT kernel: N₂ at 77 K on silica, cylindrical pores, nonlinear density functional theory (NLDFIT) equilibrium model). Pore volumes were estimated by the *t*-plot method. SEM and TEM observations were performed using a Hitachi S-3600N and a Jeol JEM-EX2000 operating at 5 kV and 200 kV, respectively. IR spectra were collected on a Thermo Fisher Scientific Nicolet Avatar-360 FT-IR spectrometer using an attenuated total reflection attachment. UV–vis absorption and fluorescence emission spectra were obtained using Jasco V-670 and FP-6500 spectrometers, respectively. XPS was recorded with an ULVAC Quantera SXM using Al K α as the X-ray source. The charge neutralization function was employed to compensate for the charge built up on solid samples by X-ray irradiation. Binding energies were referenced to In_{3d_{5/2}} at 444.4 eV from indium oxide (In₂O₃). XAFS measurements at Ru K-edge and Re L_{III}-edge were conducted by a quick XAFS (QXAFS) method in transmission mode at BL01B1 of SPring-8. X-rays stemming from synchrotron were monochromatized by Si(311) at Ru or Si(111) Re double-crystal monochromator, and the monochromator was quickly rotated within ~6 min for the measurement of a QXAFS spectrum. XAFS measurements at Ir L_{III}-edge were conducted at 30 K by a step scan method in transmission mode at BL-12C of KEK-PF using Si(111) double-crystal monochromator. An ion chamber was used to detect *I*₀ (intensity of incident X-rays), and another one placed behind the samples was used to detect *I* (intensity of transmitted X-rays). Background subtraction was performed with Autobk and Spline smoothing algorithm.³⁸ The *k*³-weighted EXAFS oscillations were Fourier transformed into *R*-space.

Synthesis of 2-Bromo-5-(triisopropoxysilyl)pyridine (2). A 500 mL three-neck flask connected to a condenser was charged with a stir bar, 2-bromo-5-iodopyridine (8.0 g, 28.2 mmol), [Rh(cod)-(CH₃CN)₂]BF₄ (0.11 g, 0.28 mmol), and *n*-Bu₄NI (12.5 g, 33.8 mmol). Dry DMF (150 mL), dry Et₃N (24 mL), and triisopropoxysilane (8.7 g, 42.3 mmol) were added. The reaction mixture was stirred at 100 °C for 24 h. After cooling to room temperature, the reaction mixture was evaporated, extracted with diethyl ether, and filtered, and then the solvent was completely evaporated. The residue was purified by silica gel column chromatography (eluent: hexane/CH₂Cl₂ = 1:1 to 1:4) to give **2** (7.0 g, 69%) as a light yellow oil. IR (neat): ν_{\max} 2974, 2933, 2895, 1562, 1539, 1446, 1383, 1371, 1286, 1174, 1117, 1074, 1043, 1016, 891, 872, 827, 762 cm⁻¹; ¹H NMR (400 MHz, CDCl₃) δ 1.18 (d, *J* = 6.2 Hz, 18H), 4.25 (septet, *J* = 6.2 Hz, 3H), 7.44 (d, *J* = 7.8 Hz, 1H), 7.74 (dd, *J* = 1.8, 7.8 Hz, 1H), 8.53 (d, *J* = 1.8 Hz, 1H); ¹³C NMR (100 MHz, CDCl₃) δ 25.4, 65.9, 127.5, 127.6, 144.3, 144.7, 155.7. FI-HRMS *m/z* calcd for C₁₄H₂₄BrNO₃Si (M⁺): 361.0709; found: 361.0710.

Synthesis of 5,5'-Bis(triisopropoxysilyl)-2,2'-bipyridine (3). A 1 L three-neck flask connected to a condenser was charged with a stir bar, **2** (10.0 g, 27.6 mmol), bis(tributyltin) (8.0 g, 13.8 mmol), and dry *m*-xylene (200 mL). Pd(PPh₃)₄ (0.5 g, 0.45 mmol) was added, and reaction mixture was stirred at 130 °C for 40 h. The resulting mixture was cooled down to room temperature and evaporated to remove solvent. The residue was purified by silica gel column chromatography (eluent: CH₂Cl₂ to EtOAc/hexane = 1:10). The obtained orange-yellow solid (5.0 g) was dissolved in acetonitrile (50 mL) and extracted with hexane (500 mL). The hexane solution was treated with activated carbon (3.0 g) for 10 min, filtered, and evaporated to give **3** (4.56 g, 59%) as a light yellow solid. IR (neat): ν_{\max} 2972, 2929, 2885, 1579, 1524, 1454, 1381, 1369, 1352, 1286, 1223, 1173, 1113, 1028, 1016, 889, 872, 843, 756, 737 cm⁻¹; ¹H NMR (400 MHz, CDCl₃) δ 1.24 (d, *J* = 6.0 Hz, 6H), 4.31 (septet, *J* = 6.2 Hz, 1H), 8.09 (dd, *J* = 1.6, 8.0 Hz, 2H), 8.40 (d, *J* = 7.3 Hz, 2H), 8.92 (s, 2H); ¹³C NMR (100 MHz, CDCl₃) δ 25.5, 65.8, 120.4, 128.6, 143.7, 1548, 157.0. FI-HRMS *m/z* calcd for C₂₈H₄₈N₂O₆Si₂ (M⁺): 564.3051; found: 564.3041.

Synthesis of BPy-PMO. A 300 mL one-neck flask was charged with a stir bar, octadecyltrimethylammonium chloride (C₁₈TMACl: 2.43 g, 6.98 mmol), 6 N NaOH solution (0.77 mL), and distilled water (132 mL). The mixture was heated at 50 °C. A solution of precursor **3** (2.97 g, 5.26 mmol) in ethanol (5 mL) was directly added to the surfactant solution through the pipet at a constant speed (2.0 mL/h

for initial 1 h, then 2.5–3.0 mL/h) using a syringe-pump system under vigorous stirring at 50 °C (Figure S1). The white suspension was then sonicated for 2 h with stirring condition at 50 °C. The mixture was stirred for another 3 days and continued heating at 50 °C for 3 days under static conditions. Then, the resulted precipitation was filtered and washed with distilled water, affording as-made bipyridine-bridged PMO. The as-made sample (2.39 g) was added into the distilled water (433 mL) in the presence of C₁₈TMACl (8.70 g) again to increase condensation degree of organosilica framework. The mixture was heated at 95 °C for 24 h under static conditions. After filtration, as-made sample (1.56 g) with thermal treatment was extracted with acidic ethanol solution (a mixture of 2 N HCl solution (7.2 mL) and ethanol (260 mL)) at room temperature for 12 h to give BPy-PMO as a white powder (1.39 g, 3.18 mmol BPy/g).

Synthesis of Ru(bpy)₂(BPy-PMO). A 200 mL three-neck flask connected to a condenser was charged with a stir bar, BPy-PMO (300 mg), and Ru(bpy)₂Cl₂·2H₂O (300 mg, 0.57 mmol). After addition of dry ethanol (60 mL), the reaction mixture was stirred at 90 °C for 24 h. The resulting precipitate was filtered and washed with CH₂Cl₂ to give Ru(bpy)₂(BPy-PMO) as an orange powder (319.9 mg, Ru content: 0.20 mmol/g).

Synthesis of Ir(ppy)₂(BPy-PMO). A 50 mL two-neck flask connected to a condenser was charged with a stir bar, BPy-PMO (100 mg), and [Ir(ppy)₂Cl]₂ (176 mg, 1.88 mmol). After addition of dry CH₂Cl₂ (33 mL), the reaction mixture was stirred at 45 °C for 15 h. The resulting precipitate was filtered and washed with CH₂Cl₂ to give Ir(ppy)₂(BPy-PMO) as a light-orange powder (122.5 mg, Ir content: 0.26 mmol/g).

Synthesis of Ir(OMe)(cod)(BPy-PMO). A 50 mL Schlenk tube was charged with a stir bar and end-capped BPy-PMO (77.5 mg, 0.226 mmol). A solution of [Ir(OMe)(cod)]₂ (5.0 mg, 0.015 mmol Ir) in dry benzene (20 mL) was added at room temperature. The reaction mixture was stirred at room temperature for 12 h. The resulting suspension was filtered and then washed with dry benzene. The material was dried over under reduced pressure to give Ir(OMe)(cod)(BPy-PMO) as a light-gray powder (80 mg, Ir content: 0.156 mmol Ir/g).

Synthesis of Re(CO)₃Cl(BPy-PMO). A 100 mL two-neck flask connected to a condenser was charged with a stir bar, BPy-PMO (100 mg), and Re(CO)₃Cl (137 mg, 0.38 mmol). After addition of dry toluene (50 mL), the reaction mixture was stirred at 110 °C for 24 h. The resulting precipitate was filtered and washed with toluene to give Re(CO)₃Cl(BPy-PMO) as a yellow-orange powder (149.1 mg, Re content: 1.12 mmol/g).

Synthesis of Pd(OAc)₂(BPy-PMO). A 20 mL Schlenk-tube was charged with a stir bar, BPy-PMO (100 mg), and Pd(OAc)₂ (21 mg, 0.08 mmol). After addition of dry THF (10 mL), the suspension was stirred at room temperature for 24 h. The resulting precipitate was filtered and washed with THF to give Pd(OAc)₂(BPy-PMO) as a yellow powder (117.5 mg, Pd content: 0.74 mmol/g).

General Procedure for the Direct C–H Borylation of Arenes Catalyzed by Ir(OMe)(cod)(BPy-PMO). A 20 mL Schlenk-tube assembled a stir bar and a septum inlet was charged with Ir(OMe)(cod)(BPy-PMO) (0.156 mmol Ir/g, 32.0 mg, 0.005 mmol Ir) and bis(pinacolato)diboron (B₂pin₂) (84.6 mg, 0.33 mmol) and then flushed with argon. An arene (20 mmol) was added, and the mixture was stirred at 80 °C for 12 h. The mixture was diluted with diethyl ether (5 mL) and filtered through a membrane filter (0.20 μm). Solvent was removed under reduced pressure. The crude product was purified by flash silica gel column chromatography (eluent: hexane/EtOAc = 100/0 to 70/30) provided analytically pure samples. The recovered catalyst was used for next reaction in the presence of B₂pin₂ and dry benzene under same reaction condition.

Synthesis of Pt/Ru(bpy)₂(BPy-PMO). A 50 mL Schlenk-tube was charged with a stir bar and K₂PtCl₆ (64 mg, 0.15 mmol). After addition of degassed distilled water (24 mL), Ru(bpy)₂(BPy-PMO) (100 mg) was added to this solution under argon flow. The suspension was stirred at 80 °C for 24 h. The resulting precipitate was filtered and washed with ethanol to remove any unreacted platinum precursor, affording Pt/Ru(bpy)₂(BPy-PMO) as a dark-brown powder (123.5

mg, Pt content: 0.10 mmol/g). S_{BET} = 570 m²/g, V_p = 0.19 cc/g, d_{DFT} = 2.7 nm.

Evaluation of Photocatalytic Hydrogen Evolution. The photocatalysis test was carried out using a glass-enclosed gas-circulation and gas-evacuation system. The vessel was loaded with Pt/Ru(bpy)₂(BPy-PMO) (10 mg, 110 μmol Pt, 1.63 μmol Ru) suspended in acetate buffer solution (25 mM, pH 4.2, 40 mL) containing EDTA (1.0 mM), followed by irradiation of visible light (>385 nm) from above using high-power xenon lamp. Producing hydrogen was detected by gas chromatography. Amount of hydrogen was plotted against irradiation time.

■ ASSOCIATED CONTENT

📄 Supporting Information

Detailed experimental procedure and Figures S1–S31. This material is available free of charge via the Internet at <http://pubs.acs.org>.

■ AUTHOR INFORMATION

Corresponding Author

inagaki@mosk.tytlabs.co.jp

Present Address

◆ Graduate School of Medicine, Dentistry and Pharmaceutical Sciences, Okayama University, Tsushima-Naka, Kita-ku, Okayama 700–8530, Japan

Author Contributions

▽ These authors contributed equally.

Notes

The authors declare no competing financial interest.

■ ACKNOWLEDGMENTS

The authors thank Dr. Tetsu Ohsuna (Toyota Central R&D Laboratories, Inc.) for TEM observations and Ms. Naoko Takahashi (Toyota Central R&D Laboratories, Inc.) for XPS measurement. The authors also thank Mr. Syuji Kajiya and Mr. Kenichi Yagi (Toyota Central R&D Laboratories, Inc.) for FI-HRMS and ESI-HRMS measurement. XAFS measurements were performed at SPring-8 (2012A1014) and Photon Factory, KEK (2013G222).

■ REFERENCES

- (1) Noyori, R. *Asymmetric Catalysis in Organic Synthesis*; John Wiley & Sons Ltd: New York, 1994; pp16–94.
- (2) (a) Amouyal, E. In *Homogeneous Photocatalysis*; Chanon, E., Ed.; John Wiley & Sons Ltd: New York, 1997; pp263–307. (b) Nicewicz, D. A.; MacMillan, D. W. C. *Science* **2008**, *322*, 77–80.
- (3) (a) Huang, J.; Zhu, F.; He, W.; Zhang, F.; Wang, W.; Li, H. *J. Am. Chem. Soc.* **2010**, *132*, 1492–1493. (b) Raja, R.; Thomas, J. M.; Jones, M. D.; Johnson, B. F. G.; Vaughan, D. E. W. *J. Am. Chem. Soc.* **2003**, *125*, 14982–14983. (c) Karamé, I.; Boualleg, M.; Camus, J.-M.; Maishal, T. K.; Alauzun, J.; Basset, J.-M.; Copéret, C.; Corriu, R. J. P.; Jeanneau, E.; Mehdi, A.; Reyé, C.; Veyre, L.; Thieuleux, C. *Chem.—Eur. J.* **2009**, *15*, 11820–11823.
- (4) (a) Benyahya, S.; Monnier, F.; Taillefer, M.; Man, M. W. C.; Beid, C.; Ouazzani, F. *Adv. Synth. Catal.* **2008**, *350*, 2205–2208. (b) Nobre, S.; Cattoën, X.; Ferreira, R. A. S.; Man, M. W. C.; Carlos, L. D. *Phys. Status Solidi RRL* **2010**, *4*, 55–57.
- (5) (a) Li, C. *Catal. Rev.* **2004**, *46*, 419–492. (b) Maschmeyer, T.; Rey, F.; Sankar, G.; Thomas, J. M. *Nature* **1995**, *378*, 159–162. (c) Li, H.; Yin, H.; Zhang, F.; Li, H.; Huo, Y.; Lu, Y. *Environ. Sci. Technol.* **2009**, *43*, 188–194.
- (6) (a) Inagaki, S.; Guan, S.; Fukushima, Y.; Ohsuna, T.; Terasaki, O. *J. Am. Chem. Soc.* **1999**, *121*, 9611–9614. (b) Asefa, T.; MacLachlan, M. J.; Coombs, N.; Ozin, G. A. *Nature* **1999**, *402*, 867–871.

- (c) Melde, B. J.; Holland, B. T.; Blanford, C. F.; Stein, A. *Chem. Mater.* **1999**, *11*, 3302–3308.
- (7) (a) Hunks, W. J.; Ozin, G. A. *J. Mater. Chem.* **2005**, *15*, 3716–3724. (b) Hoffmann, F.; Cornelius, M.; Morell, J.; Fröba, M. *Angew. Chem.* **2006**, *118*, 3290–3328. (c) Fujita, S.; Inagaki, S. *Chem. Mater.* **2008**, *20*, 891–908.
- (8) (a) Wang, W.; Lofgreen, J. E.; Ozin, G. A. *Small* **2010**, *6*, 2634–2642. (b) Mizoshita, N.; Tani, T.; Inagaki, S. *Chem. Soc. Rev.* **2011**, *40*, 789–800.
- (9) Waki, M.; Mizoshita, N.; Tani, T.; Inagaki, S. *Chem. Commun.* **2010**, *46*, 8163–8165.
- (10) Waki, M.; Mizoshita, N.; Tani, T.; Inagaki, S. *Angew. Chem., Int. Ed.* **2011**, *50*, 11667–11671.
- (11) Grüning, W. R.; Rossini, A. J.; Zagdoun, A.; Gajan, D.; Lesage, A.; Emsley, L.; Copéret, C. *Phys. Chem. Chem. Phys.* **2013**, *15*, 13270–13274.
- (12) Gispert, J. R. *Coordination Chemistry*; Wiley-VCH Verlag: Weinheim, 2008.
- (13) Lehn, J.-M. *Supramolecular Chemistry*; VCH: Weinheim, 1995.
- (14) (a) Nunes, C. D.; Valente, A. A.; Pillinger, M.; Fernandes, A. C.; Romão, C. C.; Rocha, J.; Gonçalves, I. S. *J. Mater. Chem.* **2002**, *12*, 1735–1742. (b) Nguyen, J. V.; Jones, C. W. *Macromolecules* **2004**, *37*, 1190–1203.
- (15) (a) Minoofar, P. N.; Hernandez, R.; Chia, S.; Dunn, B.; Zink, J. I.; Franville, A.-C. *J. Am. Chem. Soc.* **2002**, *124*, 14388–14396. (b) Kumar, R.; Chen, H.-T.; Escoto, J. L. V.; Lin, V. S.-Y.; Pruski, M. *Chem. Mater.* **2006**, *18*, 4319–4327. (c) Font, J.; March, P. d.; Busqué, F.; Casas, E.; Benitez, M.; Teruel, L.; García, H. *J. Mater. Chem.* **2007**, *17*, 2336–2343. (d) Sun, L.; Mai, W.; Dang, S.; Qiu, Y.; Deng, Y.; Shi, L.; Yana, W.; Zhang, H. *J. Mater. Chem.* **2012**, *22*, 5121–5127.
- (16) Inagaki, S.; Guan, S.; Ohsuna, T.; Terasaki, O. *Nature* **2002**, *416*, 304–307.
- (17) Kapoor, M. P.; Yang, Q.; Inagaki, S. *J. Am. Chem. Soc.* **2002**, *124*, 15176–15177.
- (18) Mizoshita, N.; Goto, Y.; Kapoor, M. P.; Shimada, T.; Tani, T.; Inagaki, S. *Chem.—Eur. J.* **2009**, *15*, 219–226.
- (19) (a) Sayari, A.; Wang, W. *J. Am. Chem. Soc.* **2005**, *127*, 12194–12195. (b) Cornelius, M.; Hoffmann, F.; Fröba, M. *Chem. Mater.* **2005**, *17*, 6674–6678.
- (20) Maegawa, Y.; Inagaki, S. *Solid catalyst*, Japanese Patent, JP 2013-39764, 2013.
- (21) (a) Bezombes, J.-P.; Chuit, C.; Corriu, R. J. P.; Reyé, C. *J. Mater. Chem.* **1998**, *8*, 1749–1759. (b) Kuschel, A.; Polarz, S. *Adv. Funct. Mater.* **2008**, *18*, 1272–1280. (c) Maegawa, Y.; Waki, M.; Umamoto, A.; Shimada, T.; Inagaki, S. *Tetrahedron* **2013**, *69*, 5312–5318.
- (22) Shirai, S.; Goto, Y.; Mizoshita, N.; Ohashi, M.; Tani, T.; Shimada, T.; Hyodo, S.; Inagaki, S. *J. Phys. Chem. A* **2010**, *114*, 6047–6054.
- (23) Bracco, S.; Comotti, A.; Valsesia, P.; Chmelka, B. F.; Sozzania, P. *Chem. Commun.* **2008**, 4798–4800. (b) Comotti, A.; Bracco, S.; Valsesia, P.; Beretta, M.; Sozzani, P. *Angew. Chem., Int. Ed.* **2010**, *49*, 1760–1764.
- (24) Palmer, R. A.; Piper, T. S. *Inorg. Chem.* **1966**, *5*, 864–878.
- (25) Juris, A.; Balzani, V.; Barigelletti, F.; Campagna, S.; Belser, P.; von Zelewsky, A. *Coord. Chem. Rev.* **1988**, *84*, 85–277.
- (26) Stange, A. F.; Tokura, S.; Kira, M. *J. Organomet. Chem.* **2000**, *612*, 117–124.
- (27) (a) Lowry, M. S.; Goldsmith, J. I.; Slinker, J. D.; Rohl, R.; Pascal, R. A., Jr.; Malliaras, G. G.; Bernhard, S. *Chem. Mater.* **2005**, *17*, 5712–5719. (b) Costa, R. D.; Monti, F.; Accorsi, G.; Barbieri, A.; Bolink, H. J.; Ortí, E.; Armaroli, N. *Inorg. Chem.* **2011**, *50*, 7229–7238. (c) Goldsmith, J. I.; Hudson, W. R.; Lowry, M. S.; Anderson, T. H.; Bernhard, S. *J. Am. Chem. Soc.* **2005**, *127*, 7502.
- (28) (a) Hawecker, J.; Lehn, J.-M.; Ziessel, R. *J. Chem. Soc., Chem. Commun.* **1983**, 536–538. (b) Hawecker, J.; Lehn, J.-M.; Ziessel, R. *Helv. Chim. Acta* **1986**, *69*, 1990–2012. (c) Takeda, H.; Koike, K.; Inoue, H.; Ishitani, O. *J. Am. Chem. Soc.* **2008**, *130*, 2023–2031.
- (29) Worl, L. A.; Duesing, R.; Chen, P.; Ciana, L. D.; Meyer, T. J. *J. Chem. Soc., Dalton Trans.* **1991**, 849–858.
- (30) (a) Lu, X.; Lin, S. *J. Org. Chem.* **2005**, *70*, 9651–9653. (b) Kirchberg, S.; Tani, S.; Ueda, K.; Yamaguchi, J.; Studer, A.; Itami, K. *Angew. Chem., Int. Ed.* **2011**, *50*, 2387–2391. (c) Uehara, T. N.; Yamaguchi, J.; Itami, K. *Asian J. Org. Chem.* **2013**, *2*, 938–942.
- (31) Ding, S.-Y.; Gao, J.; Wang, Q.; Zhang, Y.; Song, W.-G.; Su, C.-Y.; Wang, W. *J. Am. Chem. Soc.* **2011**, *133*, 19816–19822.
- (32) Maishal, T. K.; Alauzun, J.; Basset, J.-M.; Copéret, C.; Corriu, R. J. P.; Jeanneau, E.; Mehdi, A.; Reyé, C.; Veyre, L.; Thieuleux, C. *Angew. Chem., Int. Ed.* **2008**, *47*, 8654–8656.
- (33) (a) Ishiyama, T.; Takagi, J.; Ishida, K.; Miyaura, N.; Anastasi, N. R.; Hartwig, J. F. *J. Am. Chem. Soc.* **2002**, *124*, 390–391. (b) Ishiyama, T.; Takagi, J.; Hartwig, J. F.; Miyaura, N. *Angew. Chem., Int. Ed.* **2002**, *41*, 3056–3058. (c) Mkhaliid, I. A. I.; Barnard, J. H.; Marder, T. B.; Murphy, J. M.; Hartwig, J. F. *Chem. Rev.* **2010**, *110*, 890–931.
- (34) Kawamori, S.; Ohmiya, H.; Hara, K.; Fukuoka, A.; Sawamura, M. *J. Am. Chem. Soc.* **2009**, *131*, 5058–5059.
- (35) Tagata, T.; Nishida, M.; Nishida, A. *Tetrahedron Lett.* **2009**, *50*, 6176–6179.
- (36) Kiwi, J.; Grätzel, M. *Nature* **1979**, *281*, 657–658.
- (37) Huang, S.; Hara, K.; Fukuoka, A. *Chem.—Eur. J.* **2012**, *18*, 4738–4747.
- (38) Ravel, B.; Newville, M. *J. Synchrotron Radiat.* **2005**, *12*, 537–541.